NUCLEATION OF FATIGUE CRACKS BY INCLUSIONS

T. Jutla*, C.E. Nicholson**, and G. Jolley***

Fatigue crack initiation studies have been carried out on a C-1.5%Mn mining steel. The dominant nucleation mechanisms in the low cycle, the intermediate cycle, and the high cycle regimes have been identified. The effect on local stress intensification by the shape and orientation of typical inclusions found in the steel has been examined using Donnell's equations for surface breaking inclusions in pure tension. The findings are related to actual SEM observations of smooth surfaced specimens subjected to cyclic stresses equivalent to the fatigue limit.

INTRODUCTION

The important role played by non-metallic inclusions, second phase particles, and cavities as potential nucleation sites for fatigue cracks has received much attention in literature (1-3). It is well recognised that the role of these metallurgical discontinuities changes as the failure life increases from low cycle to high cycle. In the low cycle regime nucleation tends to be dominated by gross plasticity effects, while in the high cycle regime nucleation tends to occur at non-metallic inclusions. The intermediate regime shows a gradual transformation from slip band controlled nucleation at the lower end of the regime to nucleation from inclusions at the upper end.

The exact knowledge of how the different metallurgical discontinuities affect the fatigue properties of a material is important. This paper summarises a detailed study (4) carried out to determine the dominant nucleation mechanisms in a C-1.5%Mn

* The Welding Institute, Abington, Cambridge, U.K.
** Health and Safety Executive, Safety Engineering Laboratories, Sheffield, U.K.
*** University of Salford, The Crescent, Manchester, U.K.

mining steel in the pure low-cycle, intermediate-cycle, and pure high-cycle regimes. The experimental observations are related to some theoretical calculations based on two dimensional elastic-stress analysis.

MATERIAL

The material used was a 38mm thick C-1.5%Mn steel plate. It was used in the hardened and tempered condition, and its chemical analysis along with some mechanical properties are given in Table 1. The steel is typical of that used for haulage and winding gear in British mines and conforms to BS 2772: 1977.

TABLE 1 – Chemical Analysis and Mechanical Properties of the Material Used.

Element	C	Si	Mn	S	P	Ni	Cr	Mo	V	Cu	B
Wt.%	0.13	0.34	1.43	0.01	0.017	0.12	0.09	0.06	<0.01	0.05	<0.005

Yield stress	510 MPa
Ultimate tensile stress	584 MPa
Vickers hardness (30kg)	203

EXPERIMENTAL

Fatigue tests were carried out using 6mm diameter "hour-glass" type push-pull specimens conforming to BS 3518: Part 3: 1963. The central region of the specimen was mechanically polished to a surface finish of 1μm in a specially adapted rig. All fatigue tests were carried out under tension-zero-tension loading. Initiation studies were carried out by interrupting the fatigue tests and examining the surface of specimens in the scanning electron microscope (SEM). Detailed experimental procedures are given in reference (4).

RESULTS

Based on SEM observations the fatigue initiation mechanisms in the C-1.5%Mn mining steel are as follows:

Low Cycle Fatigue

At extremely high plastic strain ranges (failure life less than 1500 cycles), coarse slip lines are developed in the early stages and these readily aid nucleation of fatigue cracks.

Intersection points of two slip lines have frequently shown extensive damage well before nucleation along the slip lines themselves.

As the plastic strain range is reduced, the formation of coarse slip lines is also reduced, and nucleation begins to occur at favourable points along fine slip lines and at Al_2O_3 type inclusions. At the upper end of the low cycle regime (6,000 - 10,000 cycles) nucleation and early propagation occurs by a combination of the following mechanisms;

(i) nucleation from fine slip lines alone,
(ii) nucleation from alumina inclusions due to intensification of the local stress field,
(iii) nucleation due to interaction of slip lines and debonded alumina inclusions,
(iv) nucleation from alumina inclusions under the influence of local stresses and subsequent propagation of the crack along a nearby slip line.

Stringy MnS inclusions were not observed to nucleate fatigue cracks in the whole of the low cycle regime. Al_2O_3 inclusions were found to aid both surface and subsurface nucleation particularly in the intermediate and upper regions of this regime.

Intermediate Cycle Fatigue

At the lower end of this regime regions of intense slip bands are produced along with nucleation from inclusions (generally Al_2O_3 and occasionally MnS/Al_2O_3 duplex type). The upper end of the regime tends to be dominated by the development of very fine slip lines within the individual grains, and nucleation occurrs mostly from Al_2O_3 inclusions. Occasional carbide rich areas have shown extensive localised damage around cementite particles. Individual carbides in other areas were not observed to debond or cause any nucleation of microcracks.

High Cycle Fatigue

As the applied stress amplitude approaches the fatigue limit the mechanism of nucleation shifts towards cracks initiating from inclusions and on rare occasions from second phase particles. A series of events take place before fatigue cracks are nucleated at these sites (in particular at Al_2O_3 inclusions). These events are summarised below.

(i) After about 15% of life, debonding of both MnS and Al_2O_3 inclusions occurs, Fig. 1(a).
(ii) Under progressive fatigue cycling, the debonded separation becomes more pronounced.
(iii) Inclusions which remain rigid, i.e. show little or no

initial debonding, experience internal cracking at about 40% of the life, Fig. 1(b).

(iv) Between 85% - 95% of the life microcracks are developed at the equatorial poles of the cavities produced by debonded and/or damaged inclusions, Fig. 1(c).

Events (i) and (ii) apply to both Al_2O_3 and MnS inclusions. Events (iii) and (iv) apply only to Al_2O_3 type inclusions.

TWO-DIMENSIONAL ELASTIC-STRESS ANALYSIS

From the above it is clear that non-metallic inclusions play an active role as sites for nucleation of fatigue cracks. The physical and elastic properties of the different inclusions (see Table 2) determine which ones are more active initiation sites than others. Published literature (2) indicates that physical properties lead to the development of textural stresses around individual inclusions as a result of differential thermal contractions during heat treatment processes, and elastic properties can lead to intensification of local stresses at the inclusion/matrix boundary when a far-field stress is applied to the material.

TABLE 2 - Mechanical and Physical Properties of Inclusion and Matrix Materials in a C-1.5%Mn Steel (from reference (3)).

Material	Young's Modulus, E, X 10^4 N/mm^2	Poisson's Ratio, γ	Coefficient of Thermal Expansion, X10^{-6}/°C
MnS	≈13.8	0.3	18.1
Al_2O_3	38.88	0.25	8.0
Fe_3C	20.02	0.36	12.6
Matrix	20.7	0.3	14.3

The development of textural stresses around different inclusions is extensively covered by Brooksbank and Andrews (5-7). In the following analysis only the effect of elastic properties is considered for surface breaking inclusions.

Two important works related to the assessment of elastic stress fields around inclusions are (i) a two-dimensional elastic stress field model for arbitrary elliptical shapes by Donnell (8), and (ii) a three-dimensional analysis for ellipsoidal shapes by

Goodier (9). Here only surface breaking inclusions are considered, and therefore the present analysis uses Donnell's model.

In this model, the ratio K between the elastic constants for material inside and material outside an elliptical region is considered. It assumes that Poisson's ratio is the same for both materials. When K = 0, a case of an elliptical hole is defined. When K = ∞, the elliptical region is much more rigid than the material outside. For K = 1, a region without a discontinuity is defined. The model is two-dimensional and assumes that both regions inside and outside the ellipse are of the same thickness. By varying K and the shape ratio r (=a/b), the stresses at the equatorial points (α) and the polar points (β), see Fig. 2, can be obtained for different inclusions and shapes using the equations given below.

At equatorial points, α;

$$\sigma_x = K(1-K)(P+1)[(3-P)r^2-(P-1)r]N$$

$$\sigma_y = \{[K(2-K)(3-P)^2+8(P-1)]r^2+[K^2(P-1)(3-P)+K(9-4P+3P^2)+4(P-1)]r+K(P+1)^2\}N$$

$$\tau_{xy} = 0$$

At polar points, β;

$$\sigma_x = \{[K^2(9-P^2)-K(13-4P-P^2)-4(P-1)]r-K(1-K)(P+1)(3-P)\}N$$

$$\sigma_y = K(P+1)\{[K(3+P)+(P-1)]r+(P+1)(K+r^2)\}N$$

$$\tau_{xy} = 0$$

$$\text{where, } N = \frac{\sigma}{2[4K^2P-K(3-P)(P-1)+2(P-1)]r+K(P+1)^2(r^2+1)}$$

For plane stress, $P = \frac{3-\nu}{1+\nu}$, and $K = \frac{E_{inclusion}}{E_{matrix}}$

The above equations were used to compute the stresses in the x and y directions for Al_2O_3 inclusions, MnS inclusions, Fe_3C particles, and holes for different shape factors. Stress concentration factors were then calculated by normalising the resultant stress at each pole, i.e. $\sqrt{(\sigma_x^2 + \sigma_y^2)}$, by the applied stress, σ. The results are given in Fig. 3 with the exception of Fe_3C particles which gave a stress concentration factor of 1 at both equatorial and polar points. For typical shapes of inclusions, Fe_3C particles, and holes found in the C-1.5%Mn steel, the x and y components of the stress concentration factors are schematically

shown in Fig. 4. It is seen that Al_2O_3 inclusions intensify the stress at the polar points of the inclusion/matrix boundary. For MnS inclusions the stress concentraction factor is less than unity at the polar points and is equal to unity at the equatorial points. Fe_3C particles can be considered as ineffective stress raisers since they show no increase in the stress concentration factors. Holes are seen to be the most effective stress raisers, a stress concentration factor of 3 is produced at the equatorial points. Fig. 3 also shows the effect of shape and orientation of the inclusions with respect to the stressing axis.

DISCUSSION AND CONCLUSIONS

In the low cycle regime (fatigue life $< 10^4$ cycles), metallurgical constituents are not as active nucleation sites as they are in high cycle fatigue. Macro-plasticity usually dominates the former whilst localised yielding on a microscopical scale occurs at and around the fatigue limit. Under low-cycle conditions the fatigue specimen is generally subjected to large cyclic-plastic strains and this leads to intensive formation of coarse slip-bands, which interact with inclusions and second phase particles to produce fatigue-crack nuclei at an early stage in the fatigue life. At the lower end of the intermediate-cycle range (10^4-10^5 cycles), where the bulk cyclic-plastic strains are small, nucleation occurs at plastically-induced surface discontinuities and at sites of Al_2O_3 and Al_2O_3/MnS duplex inclusions. In contrast, the upper end of the intermediate-cycle range (10^5-10^6 cycles) generally corresponds to conditions under which the bulk cyclic strain in the fatigue specimen remains within the elastic range, and all the cyclic-plastic strains are confined to small regions of local stress intensification at inclusions or second phase particles.

From the SEM observations it is clear that Al_2O_3 inclusions are responsible for nucleation of fatigue cracks in the pure high cycle regime ($>10^6$ cycles). The sequence by which these inclusions cause nucleation of fatigue cracks is clear from both physical observations and theoretical analysis. In their rigid state with full bonding to the matrix, Al_2O_3 inclusions cause stress concentration equivalent to the applied stress at the polar points of the boundary. However, observations indicate that damage occurs at the equatorial points. For an alumina inclusion to cause an increase in the stress concentration at the equatorial points, they must either break internally or debond completely from the matrix. The stress concentration factor of the acting cavity then contributes to the damage at the equatorial points (stress concentration factor = 3 for a circular hole).

MnS inclusions by virtue of their shape are ineffective nucleation sites. A cavity produced by a debonded MnS inclusion has a stress concentation factor of about 1.2, which is insignificant compared to the stress concentration factor of a

circular hole. Similarly the present analysis indicates that carbide particles do not cause nucleation of fatigue cracks since their elastic properties are similar to the matrix. They have not been observed to debond from the matrix.

ACKNOWLEDGEMENTS

The authors acknowledge financial support from the Science and Engineering Research Council and the Health and Safety Executive in the form of a CASE Research Studentship for T. Jutla. The authors would like to thank the Research Director of the Health and Safety Executive for permission to publish this paper.

REFERENCES

1. Lankford, J. and Kusenberger, F.N., Met. Trans., Vol. 4, 1973, pp 553-558.

2. Lankford, J., Int. Metals Review, Vol. 22, 1977, pp 221-228.

3. Eid, N.M.A. and Thomason, P.F., Acta Metallurgica, Vol. 27, 1979, pp 1239-1249.

4. Jutla, T., "Fatigue Crack Initiation Studies in a Carbon-Manganese Mining Steel", PhD Thesis, University of Salford, 1983.

5. Brooksbank, D. and Andrews, K.W., J. of Iron & Steel Inst., Vol. 206, 1968.

6. Brooksbank, D. and Andrews, K.W., J. of Iron & Steel Inst., Vol. 207, 1969.

7. Brooksbank, D. and Andrews, K.W., J. of Iron & Steel Inst., Vol. 210, 1972.

8. Donnell, L.H., Applied Mechanics, Theodore von Karman Anniversary Volume, 1941, pp 293-309.

9. Goodier, J.N., Trans. Am. Soc. Mech. Engrs., Vol. 55, No. 39, 1933.

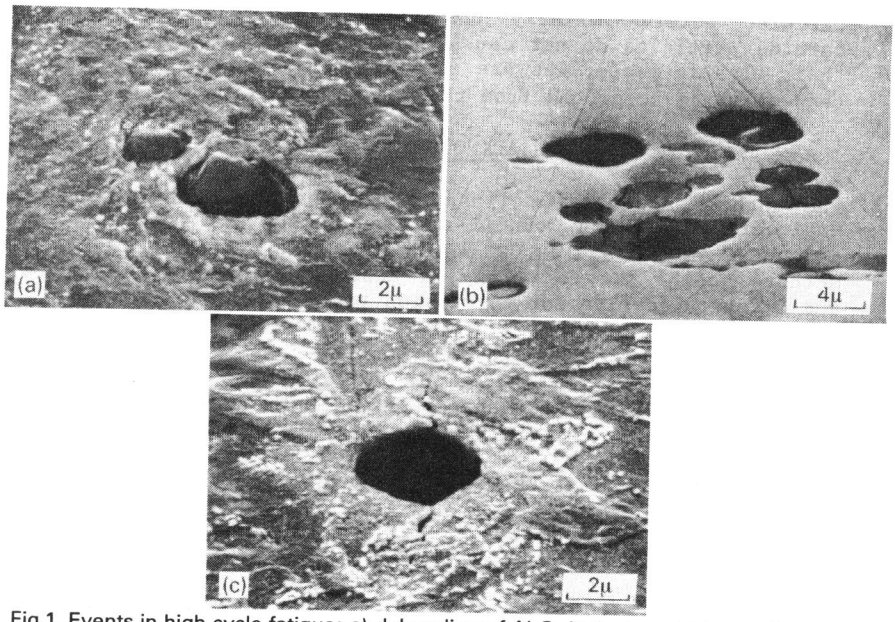

Fig.1. Events in high cycle fatigue; a) debonding of Al_2O_3 inclusions, b) internal cracking of Al_2O_3 inclusions, and c) nucleation from a cavity produced by Al_2O_3 inclusions.

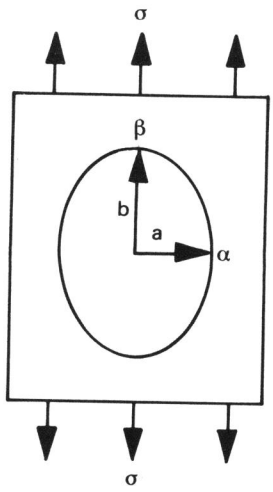

Fig.2. Description of an arbitrary elliptical shape for Donnell's model.

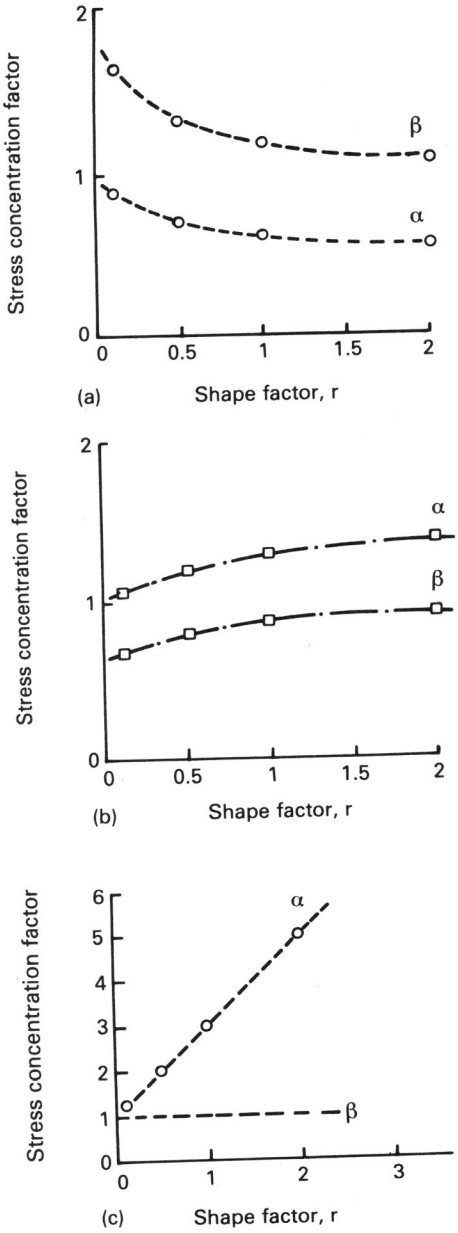

Fig.3. The effect of shape and orientation of a) Al_2O_3 inclusions, b) MnS inclusions, and c) holes on the stress concentration factor.

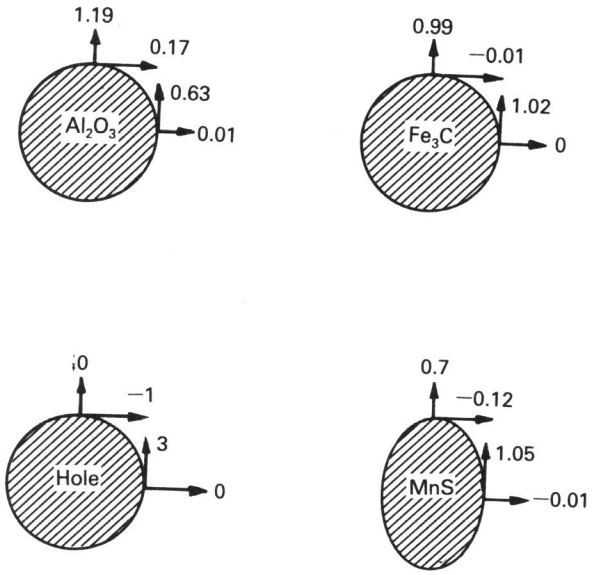

Fig.4. Stress concentration factors for typical shapes.